Inorganic Chemistry

Article

pubs.acs.org/IC

Synthesis and Characterization of $Li_{11}Nd_{18}Fe_4O_{39-\delta}$

Yao-Chang Chen,[†] Nik Reeves-McLaren,[†] Paul A. Bingham,[‡] Susan D. Forder,[‡] and Anthony R. West*[,†]

[†]Department of Materials Science and Engineering, University of Sheffield, Mappin Street, Sheffield S1 3JD, U.K.

[‡]Materials and Engineering Research Institute, Sheffield Hallam University, City Campus, Howard Street, Sheffield S1 1WB, U.K.

ABSTRACT: $Li_{11}Nd_{18}Fe_4O_{39-\delta}$ has been synthesized by the solid-state reaction of pellets, covered with powder of the same composition to avoid lithium loss, with a final reaction temperature of 950 °C. This phase has been reported previously to have various stoichiometries: $Li_5Nd_4FeO_{10}$, $Li_8Nd_{18}Fe_5O_{39}$, and $Li_{1.746}Nd_{4.494}FeO_{9.493}$. The crystal structure of $Li_{11}Nd_{18}Fe_4O_{39-\delta}$ is closely related to that reported previously for two of the other three compositions but contains extra Li and differences in Li/Fe site occupancies. Fe is present in a mixture of 3+ and 4+ oxidation states, as confirmed by Mössbauer spectroscopy. The oxygen content of $39 - \delta$ is variable, depending on the processing conditions. Samples slow-cooled in air from 800 °C are semiconducting, attributed to the presence of Fe^{4+} ions, whereas samples quenched from 950 °C in N_2 are insulating.

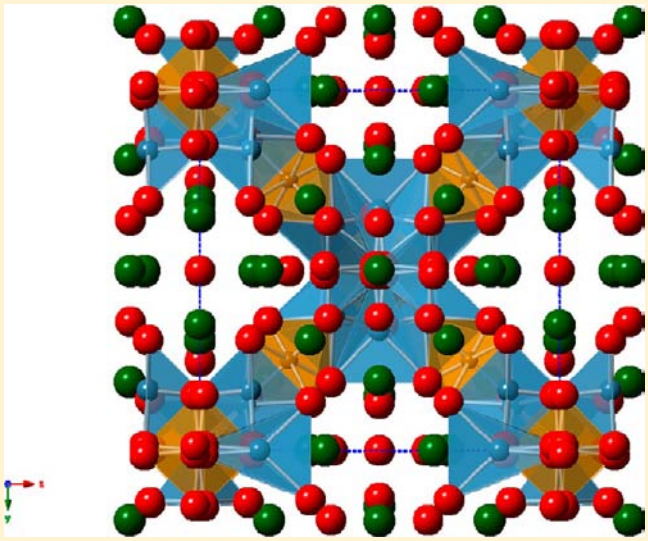

INTRODUCTION

There have been numerous reports of structurally similar phases in the systems lithium oxide−rare-earth oxide−transition-metal oxide.[1−9] Although their powder X-ray diffraction (XRD) patterns are similar and can be indexed on cubic unit cells with $a \sim 12$ Å, a number of stoichiometries have been proposed including $Li_5Nd_4FeO_{10}$,[2] $Li_8Nd_{18}Fe_5O_{39}$,[5] and $Li_{1.746}Nd_{4.494}FeO_{9.493}$[4] for the Nd system. Crystallographic studies have been reported using powder XRD and/or neutron diffraction (ND) data, and in spite of the differences in formulas, there are many similarities in the various structural reports. The structures are built of intersecting ⟨111⟩ chains made of alternating, face-sharing octahedra and trigonal prisms. These chains occupy channels within a framework of rare-earth and O atoms. While all reports agree on the general nature of the structures, they differ in the number and distribution of Li and transition-metal cations over the octahedral and trigonal-prismatic sites. The structural studies have been supported by Mössbauer spectroscopy[4−7] and magnetic measurements.[2,3,5−7]

The discrepancies in the literature concerning both the stoichiometries and structural details of these phases appear to have two possible origins. First, the synthesis of phase-pure samples is difficult by solid-state reaction in open containers. It is widely recognized that Li_2O may be lost during synthesis and, therefore, various amounts of extra Li_2O are usually added to compensate for this loss and obtain phase-pure products. This means, inevitably, that there is uncertainty from a synthetic point of view over the composition of the product phases. Second, the structures appear to contain considerable intrinsic disorder with uncertainties over the precise oxygen content and lithium/transition-metal content especially because the latter, in several cases, are disordered over certain sets of crystallographic sites. Uncertainties over the stoichiometry, together with possible cation disorder or site exchange, therefore add additional complications and uncertainties to the results of Rietveld refinements.

Our original interest in these phases followed from the discovery of garnet phases in related systems such as Li_2O−rare-earth oxide−Nb_2O_5, with formulas such as $Li_5La_3Nb_2O_{11}$, that also have large cubic unit cells, $a \sim 12.8$ Å,[10] and exhibit Li^+ ion conductivity as high as 4×10^{-5} S cm^{-1} at room temperature. In preliminary studies of the garnets, as well as the present materials, it soon became apparent that a loss of Li_2O during the synthesis was a serious problem.

There are two ways that one can tackle the difficulties of the synthesis in an open system in which the overall sample composition may be changing. First, if this approach gives products that are phase-pure and homogeneous, it is then necessary to determine their composition by some means. This can be achieved using a range of analytical techniques or, through crystal structure refinement, using XRD and/or ND, provided a satisfactory refinement can be achieved without uncertainties over site occupancies. The latter, diffraction-based approach was that adopted by previous researchers working on these materials.

Received: February 9, 2012
Published: July 23, 2012

   dx.doi.org/10.1021/ic300296s | *Inorg. Chem.* 2012, 51, 8073−8082

The second approach is to pay attention to the synthesis conditions, seek to eliminate compositional changes during synthesis, and effectively carry out reactions in a closed system. A useful approach is to work on buffered systems in which the sample reactants are pelleted and immersed in powder of prereacted but similar composition. While compositional change may be experienced by the surrounding powder during heating, the changes should be much reduced in the immersed pellets.

In cases where the composition of the desired product phase is unknown, the buffered synthesis approach can be used to investigate phase formation in a range of compositions and the results used to compile a subsolidus phase diagram showing the various phases and phase assemblages that form in different compositions. Construction of a phase diagram is also linked closely to the question of establishing equilibrium and therefore completeness of the reaction. The presentation of the results in the form of a phase diagram implies that samples have finished reacting and the resulting phases and phase mixtures are in thermodynamic equilibrium at the temperature of the reaction. A phase-diagram-based approach has several valuable characteristics, therefore. First, it requires attention to reaction conditions (temperature, time, and sometimes atmosphere) to achieve equilibrium products. Second, upon comparison of the results from a range of compositions, self-consistent results should be obtained, enabling the phase diagram to be constructed and, for instance, the likely reaction products for other compositions to be predicted. Third, for a ternary (three-component) phase diagram, single-phase compositions form the corners of subsolidus compatibility triangles and, in cases where the composition of a particular phase is uncertain, the layout of the compatibility triangles may provide a very helpful pointer toward the true composition of a particular phase.

Our approach has been to use a combination of the above strategies. Reactions were carried out under buffered conditions, avoiding loss of Li_2O and therefore making the basic assumption that the overall composition of the reaction products was the same as that of the starting materials (after loss of CO_2, H_2O, etc). This established the conditions needed to attain thermodynamic equilibrium in the reaction mixtures. The relevant subsolidus phase diagram was then determined and, in particular, self-consistent results were obtained for a range of compositions. Using this approach, it was generally possible to prepare reproducibly phase-pure samples without the need of adding extra Li_2O to compensate for a loss during the synthesis. These phase-pure samples were then used for a combination of diffraction measurements, characterization by other techniques, and electrical property measurements.

In this paper, we report the phase diagram for the system $Li_2O-Nd_2O_3-Fe_2O_3$, which shows the stoichiometry of the previously reported phase to be $Li_{11}Nd_{18}Fe_4O_{39-\delta}$. Crystallographic studies were carried out using a combination of powder XRD and ND, and the results are compared with those of previous investigations; additional characterization used Mössbauer spectroscopy and elemental analysis by scanning electron microscopy (SEM). The possibility that this phase has variable oxygen content, depending on the processing conditions, was investigated using a range of techniques, and the electrical properties were measured using impedance spectroscopy.

EXPERIMENTAL SECTION

Various compositions in the $Li_2O-Nd_2O_3-Fe_2O_3$ system were prepared by solid-state reaction. Reagents were Li_2CO_3 (Sigma-Aldrich, 99.99%, dried at 180 °C), Nd_2O_3 (Sigma-Aldrich, 99.9%, dried at 900 °C), and $Fe(C_2O_4)\cdot 2H_2O$ (Sigma-Aldrich, 99%, used as received). Samples were weighed out in stoichiometric amounts to give ∼5 g batch sizes. These were ground together with acetone using an agate mortar and pestle for ∼15 min, dried, and heated in Au foil boats at 400 °C for 2 h to drive off H_2O, initiate loss of CO_2, and commence reaction, after which they were heated to 700 °C for 12 h. Samples were then cooled, crushed, and divided into two portions; pellets were pressed, uniaxially, from one portion, and the remaining powder was used to cover the pellets, which were returned to the furnace and heated for various times and temperatures in the range 800−950 °C. This procedure was designed to avoid Li_2O loss from the pelleted samples during heating; final firing schedules were determined by trial and error to find appropriate conditions to achieve equilibrium, as indicated by no further change in the various phase assemblages with either additional heating time or increased temperature.

For phase analysis, a Siemens D5000 X-ray diffractometer with Co Kα radiation (λ = 1.78896 Å) was used with measurements over the 2θ range 5−90°. For accurate lattice parameter measurements and collection of high-resolution data for Rietveld refinement, a STOE STADI P X-ray diffractometer with a linear position-sensitive detector and Mo Kα_1 radiation (λ = 0.70926 Å) was used over the 2θ range 3−50°. Phase identification and indexing used the *WinX*^{POW} software package. Room temperature time-of-flight (ToF) ND data were collected in the backscattering detector bank ($0.2\ \text{Å} \le d \le 3.2\ \text{Å}$; resolution $\Delta d/d \sim 5 \times 10^{-3}$) on the Polaris diffractometer, at ISIS, Rutherford Appleton Laboratory, Didcot, U.K. Rietveld refinement used the EXPGUI interface for GSAS; any errors quoted are as given by GSAS.

Room temperature ^{57}Fe Mössbauer spectra were collected relative to α-Fe over the velocity range ±4 mm s^{-1} using a constant-acceleration spectrometer with a 25 mCi source of ^{57}Co in Rh. The spectra were satisfactorily fitted with three broadened Lorentzian paramagnetic doublets using the *Recoil* analysis software package. Iron and neodymium contents of grains within a pelleted sample and SEM images were obtained semiquantitatively using energy-dispersive spectroscopy (EDS) in a JEOL 6400 (JEOL Ltd., Tokyo, Japan) scanning electron microscope operating at 20 kV and a working distance of ∼14−17 mm.

The electrical properties were measured using an impedance analyzer HP 4192A with a frequency range from 5 to 10 MHz and over the temperature range 25−500 °C. Two sets of electrodes fabricated from either sputtered Au or liquid InGa were used; the atmosphere during measurement was either still air, flowing O_2, or flowing N_2. An alternating-current voltage of ∼100 mV was applied during measurements. Data were corrected for the sample geometric factor.

RESULTS AND DISCUSSION

Synthesis of $Li_{11}Nd_{18}Fe_4O_{39-\delta}$ and the Ternary Phase Diagram $Li_2O-Nd_2O_3-Fe_2O_3$. Because all previous researchers had found that the loss of Li_2O by volatilization was a serious problem for samples heated in open containers, attention was paid to establishing reaction conditions that avoided Li_2O loss during heat treatment. The great advantage in achieving this was that the final stoichiometry of the reaction mixtures should then be the same as that of the starting compositions, avoiding the necessity of adding extra, compensating amounts of Li_2O with the inevitable outcome that the final product stoichiometry would be unknown. Further, because Li_2O loss is likely to be greatest from sample surfaces, such samples may have resulting compositional gradients, thus reducing the usefulness of any "average" composition data that would be obtained by chemical analysis.

dx.doi.org/10.1021/ic300296s | *Inorg. Chem.* 2012, 51, 8073−8082

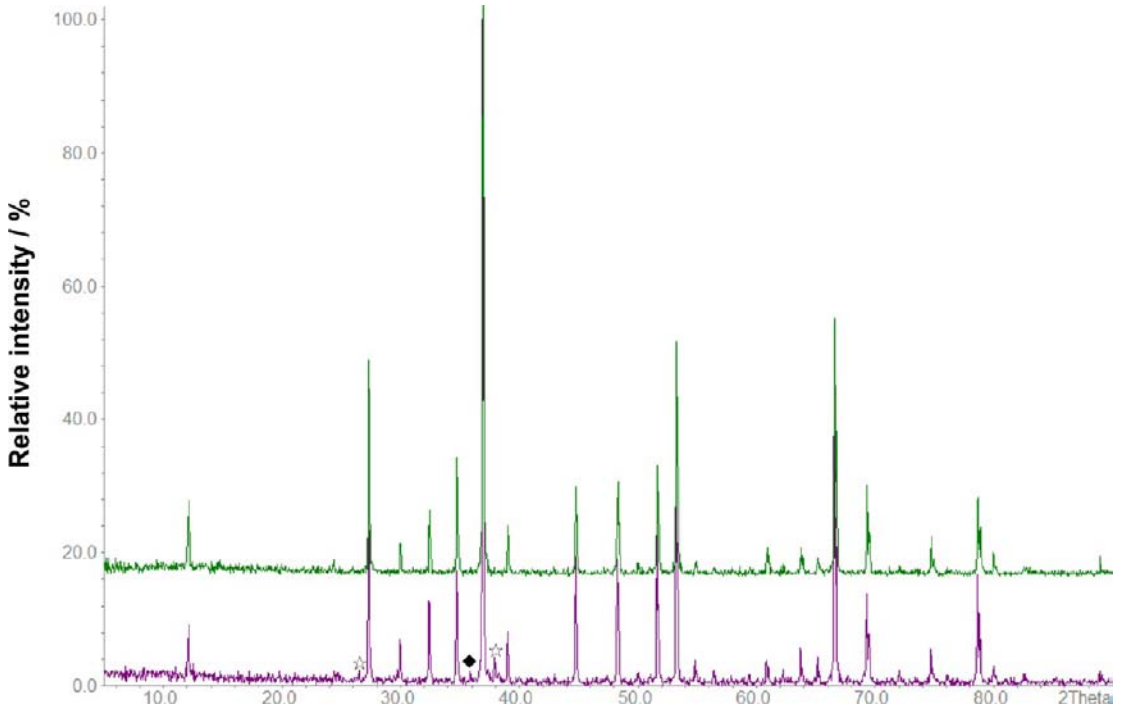

Figure 1. XRD patterns of the $Li_{11}Nd_{18}Fe_4O_{39}$ pellet (top) and covering powder (bottom): Co Kα radiation, λ = 1.78896 Å; $NdFeO_3$ marked as ☆, Nd_2O_3 marked as ◆.

In order to determine the phase diagram and prepare samples of phase-pure materials, it was therefore necessary to establish appropriate reaction conditions both to avoid Li_2O loss and to achieve equilibrium. At the outset, it was not known what the appropriate conditions should be or what was the true stoichiometry of the desired ternary phase; therefore, the synthesis procedure was somewhat iterative in that finding the appropriate reaction conditions and determining the equilibrium reaction products had to happen simultaneously. After a range of tests using different heating programs, it was found that a final heat treatment of 12−24 h at 950 °C was suitable to obtain equilibrium in the pelleted samples without evidence of significant Li_2O loss and with results that enabled construction of a self-consistent phase diagram. In this way, it was possible to prepare reproducibly phase-pure samples with composition $Li_{11}Nd_{18}Fe_4O_{39-\delta}$.

To illustrate the problems associated with Li_2O loss, XRD patterns are shown in Figure 1 for both pelleted samples and covering powder with the starting stoichiometry $Li_{11}Nd_{18}Fe_4O_{39-\delta}$ after heating at 950 °C. The pelleted sample is phase-pure, whereas the covering powder shows extra XRD peaks assigned to Nd_2O_3 and $NdFeO_3$. The presence of these phases can be explained from the phase diagram results (shown later) by loss of Li_2O during heating.

The XRD results obtained from the heating of 13 compositions at 950 °C for 12−14 h are summarized in Table 1; from these results, the subsolidus phase diagram shown in Figure 2a was constructed. This is presented as a ternary phase diagram with Fe_2O_3 as one of the components and therefore refers to the ideal situation in which all Fe is present in the 3+ oxidation state. In reality, the phase $Li_{11}Nd_{18}Fe_4O_{39-\delta}$ has an oxygen content of $39 - \delta$ that is somewhat variable, depending on the heat treatment conditions, but this had no apparent effect on the cation stoichiometries or the phase diagram; it is, therefore, valid to present data in the form of the ternary composition triangle shown in Figure 2a. Strictly, $Li_{11}Nd_{18}Fe_4O_{39-\delta}$ is a quaternary phase with four compositional variables, but for the present purposes, it can be treated as a ternary phase; it can also be described as pseudoternary.

Table 1. XRD Results of Heating Compositions in the Li_2O−Nd_2O_3−Fe_2O_3 System at 950 °C

composition	molar ratio of Li_2O−Nd_2O_3−Fe_2O_3	phases present
1 ($Li_{11}Nd_{18}Fe_4O_{39}$)	0.33:0.55:0.12	$Li_{11}Nd_{18}Fe_4O_{39}$
2 ($Li_5Nd_4FeO_{10}$)[a]	0.5:0.4:0.1	$Li_{11}Nd_{18}Fe_4O_{39}$, Li_5FeO_4, and Li_2O
3	0.33:0.6:0.07	$Li_{11}Nd_{18}Fe_4O_{39}$, $LiNdO_2$, and Nd_2O_3
4	0.4:0.4:0.2	$Li_{11}Nd_{18}Fe_4O_{39}$, $LiFeO_2$, and Li_5FeO_4
5	0.3:0.5:0.2	$Li_{11}Nd_{18}Fe_4O_{39}$, $LiFeO_2$, and $NdFeO_3$
6	0.3:0.3:0.4	$Li_{11}Nd_{18}Fe_4O_{39}$, $LiFeO_2$, and $NdFeO_3$
7	0.4:0.1:0.5	$LiFeO_2$ and $NdFeO_3$
8	0.2:0.2:0.6	$LiFeO_2$, $LiFe_5O_8$, and $NdFeO_3$
9	0.1:0.1:0.8	$LiFe_5O_8$, $NdFeO_3$, and Fe_2O_3
10 ($Li_5Nd_{18}Fe_6O_{39}$)	0.17:0.62:0.21	$Li_{11}Nd_{18}Fe_4O_{39}$, $NdFeO_3$, and Nd_2O_3
11 ($Li_{14}Nd_{18}Fe_3O_{39}$)	0.4:0.51:0.09	$Li_{11}Nd_{18}Fe_4O_{39}$, $LiNdO_2$, and Li_2O
12 ($Li_8Nd_{18}Fe_5O_{39}$)[a]	0.26:0.58:0.16	$Li_{11}Nd_{18}Fe_4O_{39}$, $NdFeO_3$, and Nd_2O_3
13 ($Li_9Nd_{18}Fe_{3.6}O_{37.62}$)[a]	0.29:0.59:0.12	$Li_{11}Nd_{18}Fe_4O_{39}$, $NdFeO_3$, and Nd_2O_3

[a]Previously reported phases in the literature.[2,5,7]

The phase diagram at 950 °C can be divided into eight compatibility triangles with one ternary phase $Li_{11}Nd_{18}Fe_4O_{39-\delta}$. This diagram differs in two respects from

dx.doi.org/10.1021/ic300296s | Inorg. Chem. 2012, 51, 8073−8082

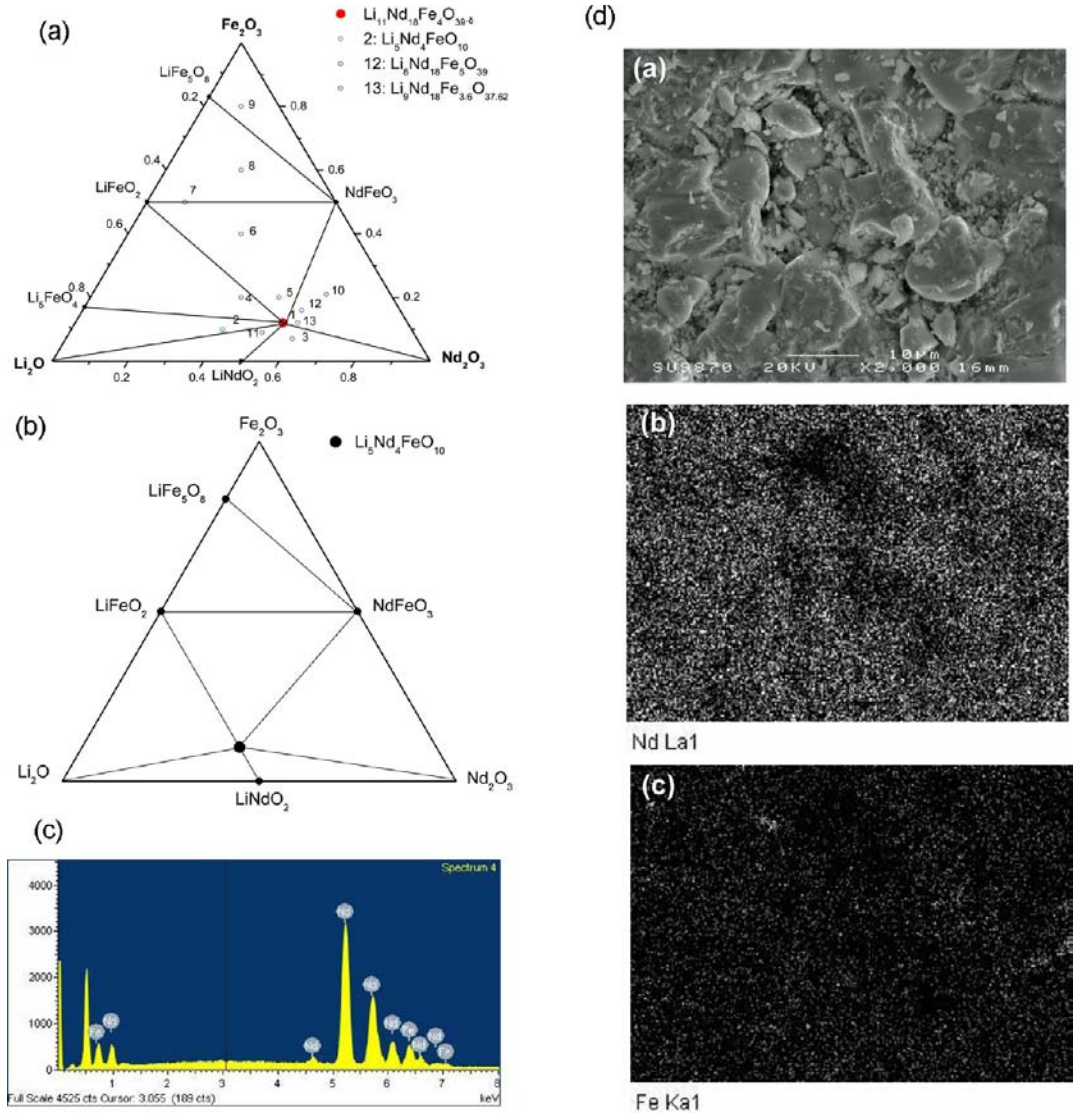

Figure 2. (a) Revised ternary phase diagram of the Li_2O–Nd_2O_3–Fe_2O_3 system. (b) Reported ternary phase diagram[2] of the Li_2O–Nd_2O_3–Fe_2O_3 system, with $Li_5Nd_4FeO_{10}$. (c) EDS spectrum of $Li_{11}Nd_{18}Fe_4O_{39}$. (d) Secondary and backscattered electron images of $Li_{11}Nd_{18}Fe_4O_{39}$.

that reported in ref 2 and shown in Figure 2b; first, a revised composition for the ternary phase is established; second, the binary phase Li_5FeO_4 is included with a modification to include those compatibility triangles that contain this phase.

Also shown in Figure 2a are the results of three compositions, 2, 12, and 13, which represent the three different compositions claimed in the literature for the ternary phase. As summarized in Table 1, each of these compositions gave three-phase mixtures when care was taken to avoid lithium loss: 2 lies in the composition triangle Li_2O–Li_5FeO_4–$Li_{11}Nd_{18}Fe_4O_{39-\delta}$; 12 and 13 lie in the composition triangle $Li_{11}Nd_{18}Fe_4O_{39-\delta}$–$Nd_2O_3$–$NdFeO_3$. It is easy to see how it is possible to switch between these different phase assemblages by varying the Li_2O content. Thus, in an open system, it is possible to start with composition 2, which upon loss of an appropriate amount of Li_2O could give essentially phase-pure composition 1; however, if too much Li_2O were lost, then assemblages of the types shown by 12 and 13 would be obtained.

In order to pinpoint the previously uncertain composition of the ternary phase $Li_{11}Nd_{18}Fe_4O_{39-\delta}$, the synthesis under equilibrium conditions of a homogeneous, single-phase product was necessary. In practice, residual amounts of secondary phases were often present, associated perhaps with incomplete mixing of the starting materials; also 2–3% of a secondary phase could easily have been present but remained undetected by routine XRD. In one of the neutron data sets, 1.9 wt % $LiFeO_2$ was detected as a minor secondary phase, although this was not seen in XRD patterns. The phase diagram results were self-consistent, however, and many of the compatibility triangles contain the phase $Li_{11}Nd_{18}Fe_4O_{39-\delta}$ as one of the corners; sufficient compositions were prepared in close proximity to this corner to help pinpoint its true composition. It was apparent from these results that the ternary phase has essentially fixed cation stoichiometry with no evidence for significant solid solution formation. This is important because, with the stoichiometries 2, 12, and 13 reported previously, an alternative interpretation could be that single-phase materials might form, as a solid solution, over a range of compositions.

The conclusion from the phase diagram studies (Figure 2a) was that the true composition of $Li_{11}Nd_{18}Fe_4O_{39-\delta}$ contains a significantly different amount of Li in comparison with the three stoichiometries reported earlier.[2,4,5] The Nd:Fe ratio of

dx.doi.org/10.1021/ic300296s | Inorg. Chem. 2012, 51, 8073–8082

Table 2. Results of Rietveld Refinement for $Li_{11}Nd_{18}Fe_4O_{39}$ Using (a) the Model from Ref 5, (b) Revisions To Allow for the Correct Iron Content, and (c) the Final Structural Model

		(a)	(b)	(c)
Nd1 24k: 0, *y*, *z*	*y*	0.3072(5)	0.3068(4)	0.3078(1)
	z	0.3075(5)	0.3073(4)	0.3062(1)
	U_{iso}/Å^2	0.0061(4)	0.0054(4)	0.0069(1)
Nd2 12f: *x*, 0, 0	*x*	0.3482(2)	0.3478(2)	0.34801(9)
	U_{iso}/Å^2	0.0039(6)	0.0023(6)	0.0032(2)
Fe1 2a: 0, 0, 0	U_{iso}/Å^2	−0.003(3)	−0.004(3)	0.0065(3)
Fe2 8e: $^1/_4$, $^1/_4$, $^1/_4$	U_{iso}/Å^2	0.016(3)	0.0007(22)	0.0027(2)
	occupancy Fe, Li	0.85, 0.15	0.75, 0.25	0.75, 0.25
Li1 16i: *x*, *x*, *x*	x	0.339(5)	0.3683	0.3733(4)
	occupancy Li, Fe	0.926, 0.074	1.0, 0	1.0, 0
	U_{iso}/Å^2	0.80(20)	0.025	0.026(1)
O1 48l: *x*, *y*, *z*	*x*	0.8651	0.8651	0.8644(1)
	y	0.8606	0.8606	0.8588(1)
	z	0.6931	0.693	0.69220(7)
	U_{iso}/Å^2	0.025	0.025	0.0099(1)
O2 6d: $^1/_4$, $^1/_2$, 0	U_{iso}/Å^2	0.025	0.025	0.0082(4)
O3 12g: *x*, 0, $^1/_2$	*x*	0.6322	0.6322	0.6305(2)
	U_{iso}/Å^2	0.025	0.025	0.0084(3)
O4 48l: *x*, *y*, *z*	*x*	0.1531	0.1531	0.1517(3)
	occupancy	$^1/_4$	$^1/_4$	0.186(2)
	y	0.015	0.015	0.0125(7)
	z	0.019	0.019	0.0123(8)
	U_{iso}/Å^2	0.025	0.025	0.01
Li2 24k: *x*, 1, *z*	*x*			0.166(2)
	z			0.142(2)
	U_{iso}/Å^2			0.006(3)
	occupancy			$^1/_6$
a/Å		11.97616(9)	11.97579(9)	11.96669(5)
space group		$Pm\bar{3}n$	$Pm\bar{3}n$	$Pm\bar{3}n$
χ^2		4.553	4.148	3.582
R_{wp}/%		9.8	9.73	2.67
R_p/%		7.76	7.46	3.43

4.5:1 may be compared with the variously reported values of 4:1[2], 4.494:1[4], and 3.6:1[5]. An additional check on the Nd:Fe ratio was obtained from EDS. A typical EDS spectrum obtained on part of a pellet of $Li_{11}Nd_{18}Fe_4O_{39-\delta}$ heated at 950 °C is shown in Figure 2c. The molar ratio of Nd:Fe, obtained from the average of 10 separate points, is 4.4(4):1, which is the same as the expected value, within errors. A secondary electron image of the heterogeneous grain structure is given in Figure 2d; in part a, the grain size varied from 1 to 15 μm. Elemental maps of Nd and Fe distribution in backscattered electron images (parts b and c) show clear evidence of a homogeneous distribution of both Nd and Fe.

Crystal Structure of $Li_{11}Nd_{18}Fe_4O_{39-\delta}$. Two crystal structures have been reported based on the stoichiometries $Li_{1.746}Nd_{4.494}FeO_{9.493}$[4] and $Li_8Nd_{18}Fe_5O_{39}$.[5] The structure reported in ref 4 has vacancies on all sites apart from Nd and, therefore, cannot be regarded as complete, at least in detail. The structure reported in ref 5 has disorder of Li and Fe over two crystallographic sites, 8e and 16i, together with a large U_{iso} for O4 with occupancy $^1/_4$. Because the phase diagram results indicated differences in both the lithium content and Nd:Fe ratio from that reported in ref 5, a cautious approach to structure determination by Rietveld refinement was required.

Initially, the model proposed in ref 5 was tested using XRD data, but a satisfactory refinement was not obtained. In particular, the U_{iso} value for Fe1 was negative, and that for Li1 [referred to as Li1 but considered to possibly contain a certain amount of Fe] was large and positive (Table 2, column a). Because it seemed likely that this model[5] contained too much Fe and given the high U_{iso} value of site Li1, the model was modified to have full occupancy of Li on this site with an initial, fixed default U_{iso} value of 0.025; the occupancy ratio of site Fe2 (primarily an Fe site but with possible partial occupancy of Li) was changed to 0.75 Fe and 0.25 Li, giving an overall iron content consistent with the stoichiometry $Li_8Nd_{18}Fe_4O_{39-\delta}$. Refinement of the revised model converged (Table 2, column b), with slight improvement of the fit between calculated and observed patterns, but Fe1 still showed a negative U_{iso} value, and it was not possible to refine the thermal parameters for Li1 and the four O positions.

Using this improved structural model as a starting point, Rietveld refinements were conducted using ND data. Background and scale factors were refined first, using a shifted Chebyschev function with six terms, followed by lattice and peak profile parameters. The profile parameters were then fixed and atomic coordinates refined in order of decreasing scattering length. Finally, thermal parameters were refined, with constraints applied to those atoms on shared sites. Preliminary refinements gave reasonable fits to the data but U_{iso} values for Li1 and O4 were large. In addition, a new site(s) for lithium was required, consistent with the expected stoichiometry. A Fourier difference map was therefore constructed; a new 24-

dx.doi.org/10.1021/ic300296s | Inorg. Chem. 2012, 51, 8073−8082

fold site (0.166, 1, 0.142) with $^1/_6$ occupancy, labeled Li2, was identified, which led to satisfactory refinement and a good fit. Careful review of all other possible sites within the structure gave only positions with unreasonably small Li−Nd distances. Final structural parameters are given in Table 2, column c, bond lengths in Table 3, and refinement profiles in Figure 3.

Table 3. Bond lengths (Å) for $Li_{11}Nd_{18}Fe_4O_{39}$ at Room Temperature

Nd1−O1	2.651(2) × 2	Fe1−O4	1.827(3) × 6
Nd1−O1	2.571(2) × 2	Fe2−O1	2.0122(8) × 6
Nd1−O1	2.479(1) × 2	Li1−O1	2.176(5) × 3
Nd1−O2	2.420(2)	Li1−04	1.958(8) × 3
Nd1−O3	2.421(1)	Li3−O1	2.35(2) × 2
Nd1−O3	3.117(2)	Li3−O1	2.63(2) × 2
Nd2−O1	2.3913(9) × 4	Li3−O4	1.85(2)
Nd2−O3	2.397(2) × 2	Li3−O4	1.57(3)
Nd2−O4	2.350(3)	Li3−Li1	1.599(8)

Attempts were made to test and refine other models for lithium site occupancies, but these were generally unsuccessful. Thus, it was suspected (see later) that site Li1 may not be fully occupied by Li but could also contain a small amount of Fe. It was, however, impossible to refine the number of Li and Fe atoms and vacancies on this site and obtain a unique solution.

The final structural model (Figure 4) for $Li_{11}Nd_{18}Fe_4O_{39-\delta}$ has Fe and mostly Li in intersecting ⟨111⟩ chains made of alternating, face-sharing $Fe1O_6$ or $Fe2O_6$ octahedra and $Li1O_6$ trigonal prisms. These chains occupy channels within a framework of $Li2O_6$, $Nd1O_9$, and $Nd2O_7$ polyhedra. The most significant revision to the model proposed in ref 5 is the addition of Li2 in partially occupied, heavily distorted 24k trigonal-prismatic sites, which share faces with $Nd2O_7$ polyhedra, edges with $Nd1O_9$, $Fe1O_6$, and $Li1O_6$ polyhedra, and corners with $Fe2O_6$ octahedra.

Li3−O bond lengths range from ∼1.6 to 2.6 Å (Table 3) compared with Li1−O and Li2−O distances of ∼1.9−2.3 Å; one Li3−Li1 distance is only ∼1.6 Å, much less than a typical Li−O bond distance. The refined model also has a relatively high U_{iso} for Li1, which may indicate that this site is less than fully occupied. The short Li3−Li1 distance may therefore

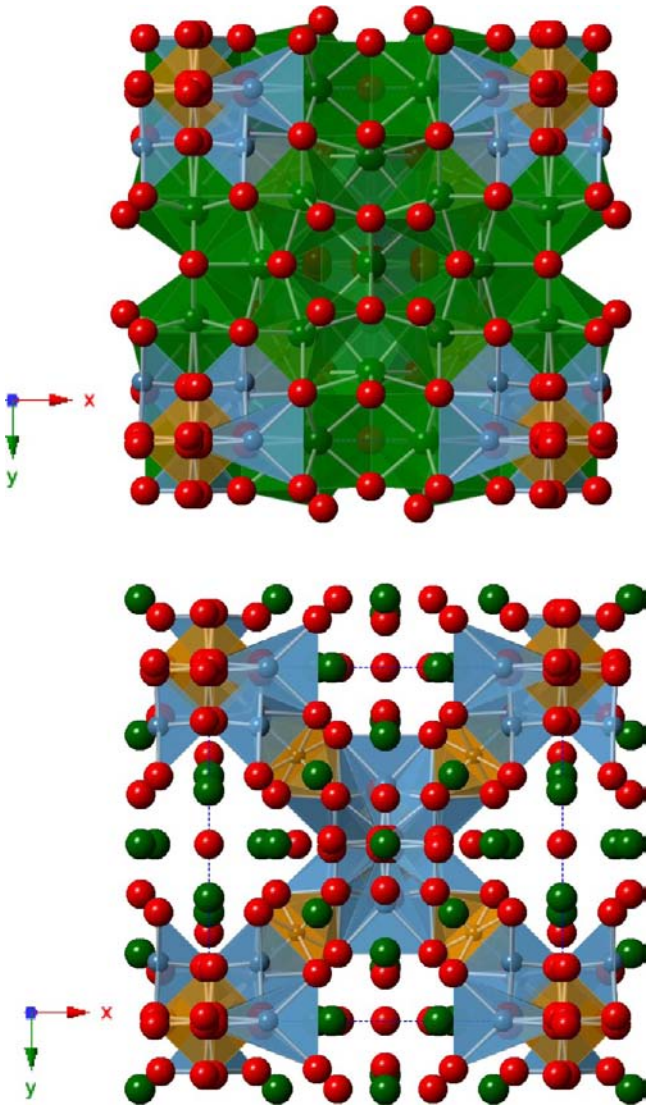

Figure 4. Refined crystal structure of $Li_{11}Nd_{18}Fe_4O_{39}$ at room temperature, showing $Fe1O_6$ and $Fe2O_6$ octahedra (orange), $Li1O_6$ and $Li2O_6$ trigonal prisms (blue), with Nd in green and O atoms as red spheres.

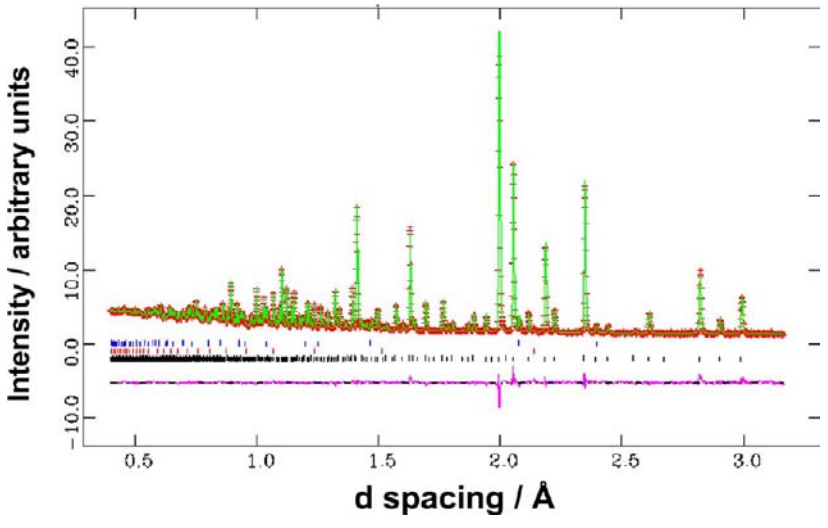

Figure 3. Observed, calculated, and difference profiles from ToF ND data for $Li_{11}Nd_{18}Fe_4O_{39}$ at room temperature.

dx.doi.org/10.1021/ic300296s | Inorg. Chem. 2012, 51, 8073−8082

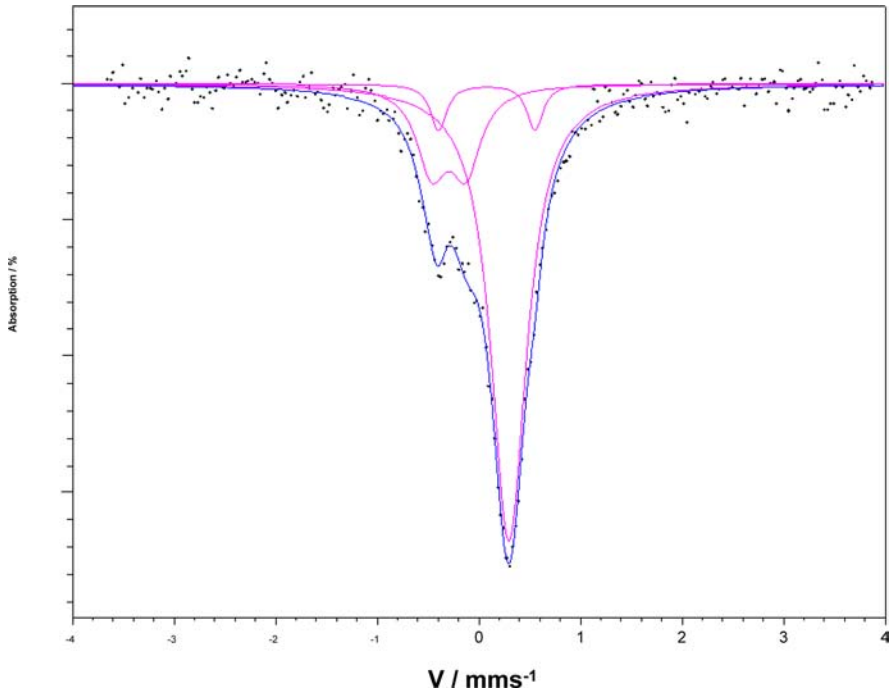

Figure 5. Fitted Mössbauer spectrum of $Li_{11}Nd_{18}Fe_4O_{39}$ obtained at room temperature.

indicate that, although Li is distributed over both sites, adjacent Li1 and Li3 sites are not simultaneously occupied. Such behavior has been observed previously in lithium orthosilicate-based systems, e.g., $Li_{4-3x}Ga_xSiO_4$,[11] where unusually short Li−Li distances were reported.

We recognize that there are residual uncertainties over the structural model listed in Table 2, column c: the Li sites and their occupancies are not necessarily finalized, given the short Li3−Li1 distances and the high thermal parameter for Li1 and also because site Li3 has an average occupancy of only $^1/_6$. For sites that contain both Li and Fe, which may or may not be fully occupied overall, refinement of the site occupancies cannot be carried out. Thus, some sites could have less than full occupancy of Li either if some sites were genuinely unoccupied or if a mixture of Li and Fe (with opposite signs of their neutron scattering lengths) occupied that set of sites. These possibilities could not be distinguished by Rietveld refinement of the ND data.

As discussed later, the oxygen content is variable depending on the processing conditions, and this appears to be accommodated by changes to the occupancy of site O4. The occupancy of this partially occupied site could not be determined with sufficient accuracy to give a precise overall oxygen content in the phase formula. From the Fe−O distances (Table 3), it appears that the smaller Fe1 site is occupied by Fe^{4+} ions and the larger Fe2 site by Fe^{3+} ions. This would give a ratio of 1:3 Fe^{4+}−Fe^{3+} in the structural formula, which is consistent, within associated errors, with the parameters extracted from the fitted Mössbauer data (later).

Mössbauer Spectroscopy. The ^{57}Fe Mössbauer spectrum of $Li_{11}Nd_{18}Fe_4O_{39-\delta}$, obtained by slowly cooling specimens in a muffle furnace in air after heating at 950 °C, is shown in Figure 5. The spectrum was fitted most satisfactorily with three Lorentzian doublets. Extracted center-shift (δ), quadrupole-splitting (Δ), and line-width (Γ) parameters are given in Table 4. It was assumed that recoil-free fraction ratio $f(Fe^{3+})/f(Fe^{4+})$ = 1. Attempts at fitting using only two broadened doublets

Table 4. Fitted Spectral Parameters for a Room Temperature Mössbauer Spectrum of $Li_{11}Nd_{18}Fe_4O_{39}$

site	center shift, δ/±0.020 mm s^{-1}	quadrupole splitting, Δ/ ±0.020 mm s^{-1}	line width, Γ/±0.020 mm s^{-1}	area/ ±2%	fit reduced χ^2
Fe^{4+} (2a)	−0.296	0.334	0.180	21.8	0.553
Fe^{3+} (8e)	0.294	0.041	0.209	71.6	
Fe^{3+} (16i?)	0.077	0.948	0.097	6.7	

produced consistently unsatisfactory results. The most intense of the three fitted doublets has a center shift of ca. 0.3 mm s^{-1}, a low quadrupole splitting of ca. 0.1 mm s^{-1} (hence, its visual appearance as a singlet), and a fitted area of ca. 72% and is consistent with Fe^{3+}.[4−7] The second doublet has a center shift of ca. −0.3 mm $^{-1}$, a quadrupole splitting of ca. 0.3 mm s^{-1}, and a fitted area of ca. 22% and is consistent with Fe^{4+}.[4−7] The third doublet, the inclusion of which in the fitting process was necessary in order to obtain satisfactory fits, has a center shift of ca. 0.1 mm s^{-1}, a quadrupole splitting of ca. 0.9 mm s^{-1}, and a fitted area of ca. 6%.

The ratio of the doublet areas in the two major sites matches, within experimental error, the occupancy ratio of 1:3 expected if the crystal structure contains Fe^{4+} ions located on the Fe1 site and Fe^{3+} ions on the Fe2 site, consistent with δ = 0 and the formula Li11$Nd_{18}Fe_4O_{39}$. The fitted parameters obtained from the third doublet would be consistent with low levels of Fe^{3+} occupying the 16i site, as has also been suggested for similar compounds.[5,6] We cannot exclude the possible existence of mixed Li/Fe occupancy on 16i sites based on the Rietveld refinement results, as indicated above.

Oxygen Content and Atmosphere Sensitivity. To determine whether $Li_{11}Nd_{18}Fe_4O_{39-\delta}$ has a variable oxygen content 39 − δ, and therefore a variable oxidation state of Fe, depending on the sample history, a sample of $Li_{11}Nd_{18}Fe_4O_{39-\delta}$

dx.doi.org/10.1021/ic300296s | Inorg. Chem. 2012, 51, 8073−8082

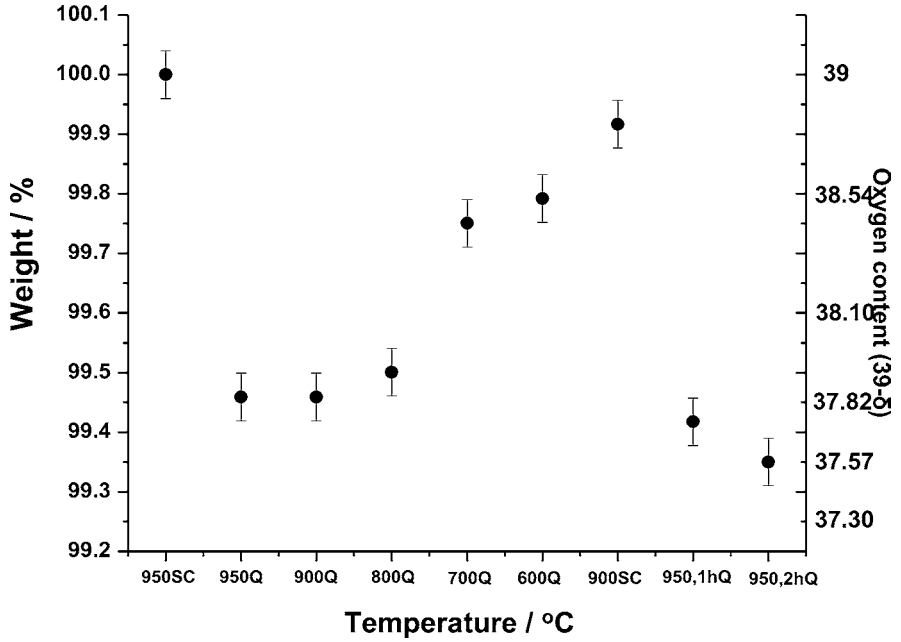

Figure 6. Weight of a $Li_{11}Nd_{18}Fe_4O_{39-\delta}$ pellet after heating sequentially at various temperatures in air: Q, quench; SC, slow cool.

was heated at 950 °C and then cooled slowly to room temperature. The same sample was reheated at different temperatures for different times, quenched by dropping into liquid N_2, and weighed. The results are summarized in Figure 6 and show reversible changes that are most likely attributable to oxygen loss/gain.

The starting weight was taken as that of the sample slow-cooled in air from 950 °C; subsequent data points refer to samples reheated isothermally at progressively lower temperatures followed by quenching. The sample was then reheated to 900 °C in air and cooled slowly; the original sample weight was almost regained. Subsequent tests showed the essential reversibility of the oxygen loss and gain. There may be a net downward drift in the weight data as shown by a comparison of the initial sample weight and that after reheating at 900 °C and also by the final two data points showing the effect of time at 950 °C. The right-hand axis of Figure 6 is calibrated to assume that the starting material had an oxygen content of 39, i.e., $\delta = 0$; allowing for a small loss of Li_2O during the experiments, the oxygen loss in samples quenched from high temperatures appears to reduce to a value of ~38, which would correspond to a mixture of 3+ and 2+ oxidation states for Fe.

Tests were also carried out to check the sensitivity of samples to atmospheric attack at room temperature. Samples were prepared, left open to the atmosphere at room temperature, and then weighed periodically. Samples that were given a final slow cool from 950 °C were found to be relatively insensitive to atmospheric attack, as shown by no major changes in weight. However, samples quenched from 950 °C showed a gradual increase in weight over a period of several days, indicating that these oxygen-deficient samples were sensitive to the atmosphere. It was not determined whether the increase in weight was due to uptake of O_2 or H_2O/CO_2.

Electrical Properties of $Li_{11}Nd_{18}Fe_4O_{39-\delta}$. Pellets of $Li_{11}Nd_{18}Fe_4O_{39-\delta}$ sintered at 950 °C in air and then given a range of other heat treatments were used for electrical property measurements by impedance spectroscopy. It was found that the impedance data generally fell into one of two groups: those for samples heated in air and those heated in N_2 at high temperatures. The N_2 samples were much more resistive than the air samples.

Typical impedance data sets are shown in Figures 7 and 8. Generally, two arcs were observed in the impedance complex plane plots (a), and it was possible to extract bulk sample conductivities from the intercept of the high-frequency arc on the real Z' axis. These data are plotted in conventional Arrhenius format in Figure 9.

For samples heated in air (Figure 7), the impedance complex plane plots (a) show two approximately semicircular arcs; replotting the same data as spectroscopic plots of capacitance C' (c) shows two plateaux. The high-frequency plateau with a value of $\sim(2-3) \times 10^{-12}$ F cm^{-1} represents the bulk response of the sample with a permittivity of ~20−30. The low-frequency plateau has an approximate value of 10^{-6} F cm^{-1} and is associated with the sample−electrode interfacial response. There was no evidence of any intermediate frequency plateaux such as could be associated with a grain boundary impedance.

Impedance data for samples heated in N_2 at 950 °C (Figure 8) also showed two arcs in the impedance complex plane plot (a), but the low-frequency arc had a much smaller resistance than the high-frequency arc. The C' spectroscopic plots (c) again showed a high-frequency plateau, representing the bulk response, and an increasing capacitance at lower frequencies, which did not attain values as high as those shown in Figure 7. These data also represented the electrode−sample response, but the associated impedance had only a minor effect on the overall electrical properties.

The C' data for the sample heated in N_2 are typical of a material that is a modest electronic conductor in which the low-frequency capacitance represents an interfacial impedance at the sample−electrode contact, possibly associated with the formation of a Schottky barrier. For the samples heated in air, the capacitance data are much higher (Figure 7c) but, nevertheless, are still attributed to electronic conduction rather than ionic conduction of either O^{2-} or Li^+ ions. Thus, the impedance complex plane plots (Figure 7a) show no evidence

dx.doi.org/10.1021/ic300296s | Inorg. Chem. 2012, 51, 8073−8082

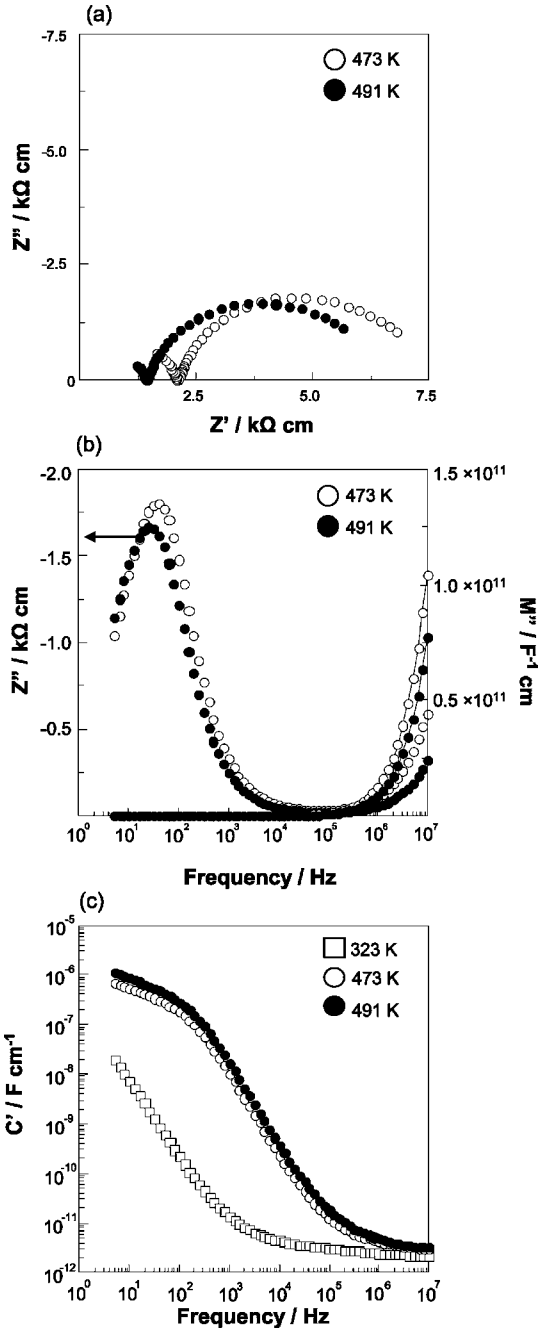

Figure 7. Impedance data for $Li_{11}Nd_{18}Fe_4O_{39}$ heated at 950 °C in air with relative density 83%: (a) impedance complex plane plots; (b) $-Z''$ and M'' spectroscopic plots; (c) C' plots.

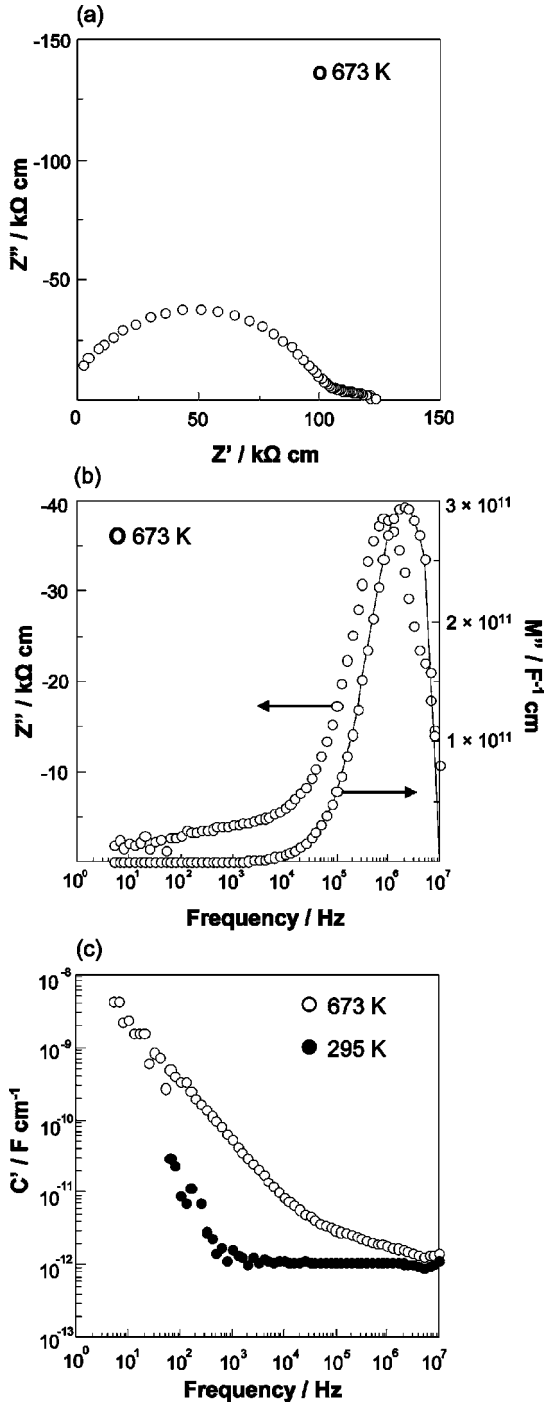

Figure 8. Impedance data for $Li_{11}Nd_{18}Fe_4O_{39}$ heated at 950 °C in N_2 atmosphere with relative density 80%: (a) impedance complex plane plots; (b) $-Z''$ and M'' spectroscopic plots; (c) C' plots.

of any low-frequency effects such as an inclined Warburg spike. In addition, the low-frequency arc was found, in a separate experiment, to be insensitive to the atmosphere, which was switched between air, O_2, and N_2, during measurements; if oxide ion conduction had been responsible for the measured conductivity, then certainly it would be expected that the low-frequency arc would be sensitive to P_{O_2} in the atmosphere. We therefore attribute the low-frequency arcs to the formation of a Schottky barrier at the sample−electrode interface and, in particular, to a depletion layer at the sample surface.

The marked difference in Arrhenius plots between N_2 and air samples can be readily interpreted in terms of an electronic mechanism of conduction. The results are shown in Figure 9 for samples given a range of heat treatments. The sample with the lowest conductivity and highest activation energy is that quenched from 950 °C after heating in N_2. Upon subsequent reheating of the same sample at 400 °C in air, a small increase in the conductivity occurred. All of the other samples, which were heated in air and cooled from 950, 800, and 500 °C, or the sample heated initially in N_2, quenched, and subsequently reheated at 800 °C in air had much higher conductivity. All of these samples had conductivity of $\sim 10^{-6}$ S cm^{-1} at room temperature with activation energy of ~0.47 eV. Because these samples contain a mixture of Fe^{3+} and Fe^{4+}, their conductivity is

dx.doi.org/10.1021/ic300296s | Inorg. Chem. 2012, 51, 8073−8082

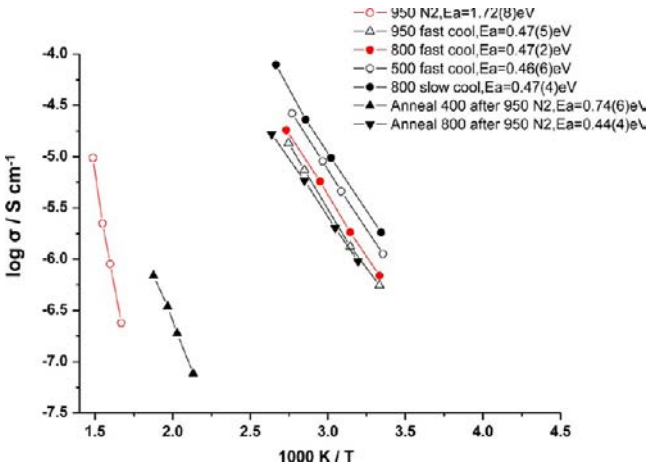

Figure 9. Arrhenius plots of $Li_{11}Nd_{18}Fe_4O_{39}$ heated in N_2 or air at various temperatures.

attributed to the presence of Fe^{4+} ions and, therefore, to a hole conduction mechanism. Fe^{4+} ions are absent from the sample heated in N_2 at 950 °C and quenched, and the residual conductivity is associated with Fe^{3+} and/or Fe^{2+} ions. Some Fe^{4+} ions may have been reintroduced upon reheating of the sample at 400 °C in air, as shown by its increased conductivity, but the extent of reoxidation was incomplete.

CONCLUSIONS

The pseudoternary phase diagram for the system Li_2O–Nd_2O_3–Fe_2O_3 has been studied and the composition of the ternary phase $Li_{11}Nd_{18}Fe_4O_{39-\delta}$ established by careful avoidance of lithium loss during synthesis. This phase has been reported previously to have the stoichiometries $Li_5Nd_4FeO_{10}$, $Li_8Nd_{18}Fe_5O_{39}$, and $Li_{1.746}Nd_{4.494}FeO_{9.493}$. The crystal structure of $Li_{11}Nd_{18}Fe_4O_{39-\delta}$ is closely related to that reported previously for two of the other three compositions but contains extra lithium in heavily distorted trigonal-prismatic sites and differences in Li/Fe site occupancies. The oxygen content δ is variable, depending on the processing conditions; Mössbauer spectroscopy, ND data, and impedance spectroscopy data indicate the presence of mixed Fe^{3+} and Fe^{4+} in samples slow cooled in air. Conduction in the samples is believed to be primarily electronic in nature and increases greatly in samples that contain Fe^{4+} ions.

AUTHOR INFORMATION

Corresponding Author

*E-mail: a.r.west@sheffield.ac.uk.

Notes

The authors declare no competing financial interest.

ACKNOWLEDGMENTS

We thank the Engineering and Physical Sciences Research Council for financial support.

REFERENCES

(1) Mazza, D.; Abbatista, F.; Vallino, M.; Ivaldi, G. *J. Less-Common Met.* **1985**, *106* (2), 277–285.
(2) Ban, I.; Drofenik, M.; Suvorov, D.; Makovec, D. *Mater. Res. Bull.* **2005**, *40* (10), 1856–1863.
(3) Frampton, P. P. C.; Battle, P. D.; Ritter, C. *Inorg. Chem.* **2005**, *44* (20), 7138–7142.
(4) Drofenik, M.; Ban, I.; Makovec, D.; Hanzel, D.; Golobic, A.; Golic, L. *J. Solid State Chem.* **2007**, *180* (1), 2–7.
(5) Dutton, S. E.; Battle, P. D.; Grandjean, F.; Long, G. J.; Oh-ishi, K. *Inorg. Chem.* **2008**, *47* (23), 11212–11222.
(6) Dutton, S. E.; Battle, P. D.; Grandjean, F.; Long, G. J.; van Daesdonk, P. A. *Inorg. Chem.* **2009**, *48* (4), 1613–1623.
(7) Battle, P. D.; Dutton, S. E.; van Daesdonk, P. A. *J. Solid State Chem.* **2010**, *183* (7), 1620–1624.
(8) Battle, P. D.; Dutton, S. n. E.; Thammajak, N.; Grandjean, F.; Sougrati, M. T.; Long, G. J.; Oh-ishi, K.; Nakanishi, S. *Inorg. Chem.* **2010**, *49* (13), 5912–5922.
(9) Battle, P. D.; Dutton, S. n. E.; Grandjean, F.; Long, G. J.; Thammajak, N.; Wisetsuwannaphum, S. *J. Solid State Chem.* **2011**, *184* (9), 2580–2587.
(10) Thangadurai, V.; Kaack, H.; Weppner, W. J. F. *J. Am. Ceram. Soc.* **2003**, *86* (3), 437–440.
(11) Smith, R. I.; West, A. R. *J. Mater. Chem.* **1991**, *1* (1), 91–96.